Materials and Structures (2025) 58:235
https://doi.org/10.1617/s11527-025-02754-2

RILEM TC REPORT

Examining reproducible mix design, fresh and mechanical properties of ground granulated blast furnace slag-based alkali-activated concrete (GGBFS-based AAC): results of an interlaboratory study of RILEM TC 294-MPA

Patricia Kara De Maeijer · Guang Ye · Zhenming Li · Kruthi Kiran Ramagiri · Geert De Schutter · Yubo Sun · Frank Dehn · Arkamitra Kar · Juho Yliniemi · Yuwei Ma · Kazuo Ichimiya · Giulia Masi · Quoc Tri Phung · Wei Sha

Received: 25 February 2025 / Revised: 25 July 2025 / Accepted: 2 August 2025

Abstract This report presents a meticulous synthesis of collaborative interlaboratory research conducted within the purview of the RILEM Technical Committee 294-MPA, with two expert groups named RRT1 and RRT2, and encompassing ten participants from Belgium, China, Finland, India, Italy, Japan, the Netherlands, and the United Kingdom. The RRT1 expert group mainly focused on the ground granulated blast furnace slag-based alkali-activated concrete (GGBFS-based AAC) mix design and mechanical properties. In turn, the RRT2 expert group focused on the fresh properties of GGBFS-based AAC. The investigation, conducted between 2020 and 2024, aimed to establish globally reproducible mix design and mixing protocols for GGBFS-based AAC. Developed by the RRT1 and RRT2 expert groups, these protocols have emerged through iterative experiments followed by a comprehensive interlaboratory study. The outcomes highlight the reliable production of GGBFS-based AAC across participants, with minor deviations in fresh and mechanical properties that are largely consistent with those observed in Portland cement concrete (PCC). The primary objective of the developed GGBFS-based AAC mix design was to achieve a defined consistence class S4, while targeting a compressive strength threshold of approximately 50 MPa at 28 days. This objective was effectively realized, with the average compressive strength values reaching 56 MPa at 28 days and 64 MPa at 720 days. While the average splitting tensile strength stabilized at 3.2 MPa over the 720 day period. These findings underscore the growing importance of AAC within the construction sector, particularly due to its reproducible and reliable experimental results, as the industry increasingly shifts toward more sustainable alternatives to traditional cement-based materials.

RILEM TC footnote: This study was performed within the framework of the RILEM TC 294-MPA "Mechanical properties of alkali-activated concrete" by RRT1 and RRT2 expert groups from August 2020 to March 2024. This TC Report was internally reviewed and approved by the RILEM TC 294-MPA Active Members by 26th November 2024 that concluded its activities on 27th September 2024.

TC 294-MPA Membership:.

TC 294-MPA Chair: Guang Ye.

TC 294-MPA Deputy Chair: Frank Dehn.

TC 294-MPA Active Members: Elijah Damilola Adesanya, Rahul Attupurathu Vijayan, Susan Bernal Lopez, Farid Benboudjema, Jelle Bezemer, Maria Chiara Bignozzi, Choi Lin Chan, Boyu Chen, Ozlem Cizer, Xiaodi Dai, Vinh Dao, Geert De Schutter, Frank Dehn, Brice Delsaute, Vilma Ducman, Pujitha Ganapathi Chottemada, Meng Gao, Luise Gobel, Lucija Hanzic, Zhangli Hu, Yuyan Huang, Kazuo Ichimiya, Sri Kalyana Rama Jyosyula, Muralidhar Kamath, Fragkoulis Kanavaris, Arkamitra Kar, Patricia Kara De Maeijer, Arno Keulen, Albina Kostiuchenko, Sreejith Krishnan, Pavel Kryvenko, Maite Lacante, Georgy Lazorenko, Ning Li, Zhenming Li, Tianshi Lu, Mladena Lukovic, Tero Luukkonen, Yang Lv, Yuwei Ma, Alastair Marsh, Giulia Masi, Stijn Matthys, Luiz Miranda de Lima, Shravan Muthukrishnan,

Published online: 26 August 2025

Keywords Alkali-activated concrete (AAC) · Ground granulated blast furnace slag (GGBFS) · Fresh properties · Mechanical properties

1 Introduction

Alkali-activated concrete (AAC) represents a significant advancement in construction material research, potentially offering an alternative to Portland cement concrete (PCC) [1, 2]. This manuscript presents a comprehensive synthesis derived from a collaborative interlaboratory research conducted by ten participants from eight countries. The objective of this interlaboratory research was to analyse the characteristics of ground granulated blast furnace slag (GGBFS)-based AAC and its potential as a viable construction material. This collaborative endeavour strategically integrated the expertise of participants to scrutinize the intricate mechanical and fresh properties of GGBFS-based AAC.

The mechanical efficacy of AAC largely pivots on intricate mix proportions, encompassing critical elements such as the type of alkali activator [3], alkali content [4], water-to-solid (w/s) ratio

Mariya Nedeljkovic, Behzad Nematollahi, Kolawole A. Olonade, Marta Palacios, Majda Pavlin, Quoc Tri Phung, John L. Provis, Francisca Puertas Maroto, Zhenxu Qian, Zhengyao Qu, Kruthi Kiran Ramagiri, Jesus Rodriguez-Sanchez, Laura Rossi, Aljosa Sajna, Marco Sirotti, Wei Sha, Caijun Shi, Stephanie Staquet, Beibei Sun, Yubo Sun, Yaxin Tao, Babak Vafaei, Jannie S. J. van Deventer, Xiaomei Wan, Frank Winnefeld, Jean Noel Yankwa Djobo, Guang Ye, Hailong Ye, Kangting Yin, Juho Yliniemi, Zengliang Yue, Minzhong Zhang, Shizhe Zhang, Zuhua Zhang, Zhengning Zhou, Xiaohong Zhu, Lea Zibret and Yibing Zuo.

P. Kara De Maeijer (✉)
Faculty of Civil and Mechanical Engineering, Riga Technical University, Riga LV-1048, Latvia
e-mail: pkdm.rtu@gmail.com

P. Kara De Maeijer
Faculty of Applied Engineering, University of Antwerp, 2020 Antwerp, Belgium

G. Ye · Z. Li
Group Concrete Modelling and Materials Behavior, Microlab/Section Materials and Environment, Department of 3MD, Faculty of Civil Engineering and Geosciences, Delft University of Technology, 2628 CN Delft, The Netherlands

Z. Li
School of Civil and Environmental Engineering, Harbin Institute of Technology, Shenzhen 518055, China

Z. Li
Guangdong Provincial Key Laboratory of Intelligent and Resilient Structures for Civil Engineering, Harbin Institute of Technology, Shenzhen 518055, China

K. K. Ramagiri
MYK Laticrete, Hyderabad, Telangana 502 329, India

G. De Schutter
Magnel-Vandepitte Laboratory, Department of Structural Engineering and Building Materials, Ghent University, 9052 Ghent, Belgium

Y. Sun
Department of Civil and Environmental Engineering, The Hong Kong Polytechnic University, Hong Kong 999077, China

F. Dehn
Karlsruhe Institute of Technology (KIT), Institute of Concrete Structures and Building Materials (IMB), DE-76131 Karlsruhe, Germany

A. Kar
Department of Civil Engineering, Birla Institute of Technology and Science-Pilani, Hyderabad, Telangana 500 078, India

J. Yliniemi
Fibre and Particle Engineering Research Unit, University of Oulu, FI-90014 Oulu, Finland

Y. Ma
Research Center for Wind Engineering and Engineering Vibration, Guangzhou University, Guangzhou 510006, China

K. Ichimiya
Department of Civil and Environmental Engineering, National Institute of Technology, Oita College, Oita 870-0152, Japan

G. Masi
Department of Civil, Chemical, Environmental and Materials Engineering, University of Bologna, 40131 Bologna, Italy

Q. T. Phung
Belgian Nuclear Research Centre (SCK CEN), 2400 Mol, Belgium

W. Sha
School of Natural and Built Environment, Queen's University Belfast, Belfast BT9 5AG, UK

[5], composition and type of precursors [6], curing duration [7], temperature [8], etc.

The mix design and control of the setting time are vital for GGBFS-based AAC, which can rapidly lose workability (often setting in less than 30 min), limiting its use in ready-mix and pumped concretes [9, 10]. The uncontrolled rapid setting is attributed to heat from the solid dissolution or the high calcium content [7]. Adjusting the AAC mix proportions, such as optimizing the calcium content or adding water, delays setting but can compromise the mechanical properties of AAC. Common admixtures for PCC may not be compatible with AAC [11], suggesting a need to explore methods for separately adding admixtures and alkali activators [12].

The multifaceted development of the mechanical properties of AAC is notably influenced by the precursor selection, activator combinations, mixing procedures and curing conditions. The intricacies in understanding the mechanical traits of GGBFS-based AAC demand extensive comparisons with PCC. Variations in activator types, proportions, and curing methods distinctly impact the hardened properties, making it challenging to derive generalized trends due to inherent variability among different AAC compositions [11, 13–15].

The curing conditions significantly dictate the strength development of AAC. While heat curing initially boosts strength of GGBFS-based AAC, it may later decrease due to microstructural inconsistencies, resulting in a less dense structure [16, 17]. The conflicting effects of humidity and lime water curing manifest differential impacts on reaction and strength development, emphasizing the importance of moisture retention and effective reaction mechanisms in fostering superior strength development [18, 19].

The strength of AAC is significantly dependent on the effective density, space-filling capacity, and binding capabilities of the main phases, C-A-S-H gel, and Mg–Al layered double hydroxides. Despite frequently attaining similar 28-day strengths and stress–strain relations in compression as PCC [15, 20], differences in long-term performance arise from differential reaction kinetics, curing temperatures, and alkalinity levels. The reactivity of raw materials significantly influences the mechanical behaviour of AAC, necessitating tailored mix designs to optimize the strength outcomes. AAC formulated with GGBFS exhibits rapid early-age strength owing to the swift dissolution of GGBFS particles, fostering a compact transition zone within the structure. Sodium silicate solutions lead to superior early strength development in AAC [19, 21]. The Na_2O_{eq}/binder (N/B) ratio is a crucial determinant, highlighting the potential of AAC to achieve strengths up to 60 MPa [22]. Meticulous regulation of parameters such as the water-to-binder (w/b) ratio is imperative to attain the desired compressive strengths in AAC, underscoring the intricate control required in its formulation.

Unlike compressive strength analysis, tensile strength assessments in AAC involve various tests, such as direct tensile, splitting tensile, and flexural tensile evaluations [23–26]. However, inconsistencies in the findings arise from factors such as precursor type, activator dosage, and curing methods, leading to conflicting conclusions [27, 28]. Although some studies suggest that GGBFS-based AAC shares similarities with PCC in terms of tensile strength, others highlight potential of GGBFS-based AAC for a better performance under certain conditions [29, 30] or indicate that GGBFS-based AAC is subjected to failure under tension [31]. Research focusing on predicting the splitting tensile strength in AAC, especially involving nanomaterials, shows promise in enhancing the mechanical properties [32, 33]. However, the inadequacy of the current design codes in fully capturing the splitting tensile strength of AAC, particularly in compositions using GGBFS, remains evident. Rossi et al. [34] underscored the complexity within alkali-activated systems, revealing the limitations of relying solely on binder types to characterize the mechanical behaviour of AAC. The diverse findings across studies emphasize the need for more comprehensive investigations considering various mix designs to accurately assess the tensile response of AAC.

Assessments of the elastic modulus in AAC indicate that its variability is influenced by several factors, including precursor material variations, types of activators, mix designs, and long-term performance under exposure conditions. Research has shown that AAC generally has a slightly lower elastic modulus compared to the strength classes of PCC when different alkali activators are used [35, 36]. Additionally, AAC containing GGBFS exhibits minimal variation in the elastic modulus relative to its compressive strength. However, the experimental results do not

align closely with the ACI Building Code 318 [37], possibly due to the presence of initial microcracks in the matrix after setting, which may reduce the elastic modulus of AAC [38]. This complexity in the AAC mix parameters and activator variations emphasizes the need for more refined models to accurately predict the elastic modulus of AAC.

In many cases, despite sporadic successful application of AAC in Australia, China, Europe, and India, achieving reliable performance is typically rare and requires extensive trial-and-error interlaboratory experimentation [39]. This reality imposes constraints on advancing the structural exploration of AAC in practical applications, thereby hindering widespread industrial applications [22]. Nonetheless, AAC is making inroads into the construction industry.

As mentioned above, there is often significant variation in the results reported in the scientific literature regarding AAC [39, 40]. Both industry and academia would benefit from an interlaboratory study, as they could increase confidence in the findings. This interlaboratory study aimed to develop globally reproducible mix designs and mixing protocols for GGBFS-based AAC with testing conducted across ten participants in eight different countries. Two TC 294-MPA expert groups, named RRT1 and RRT2, contributed to the evaluation of the fresh and mechanical properties of GGBFS-based AAC in this interlaboratory study. The RRT1 expert group focused on the mix design and mechanical properties (density, compressive and splitting tensile strengths, and elastic modulus), whereas the RRT2 expert group concentrated on fresh properties (slump, flow, and rheology). The variations in results both within and between laboratories were compared and analyzed.

2 Materials and methods

2.1 Materials

2.1.1 Raw materials

To ensure the repeatability and reproducibility of slump, flowability, and mechanical tests on AAC, and to enable valid comparisons across participants, most were required to use the same raw material. GGBFS from the same batch supplied by EcoCem Ireland was delivered to participants in Belgium, the Netherlands, Italy, Finland, and the UK. Due to high delivery costs, participants in China, India, and Japan used locally sourced GGBFS, allowing for internal comparisons of AAC properties based on different slag sources. Therefore, four sources of GGFBS were used in this study. Seven out of ten participants performed characterization of GGBFS provided samples, and their chemical composition along with other properties are summarized in Tables 1 and 2. The morphology from the SEM analysis performed by participant 7 is shown in Fig. 1. The GGFBS is comprised of angular particles without any specific shape, with a median size of 10–14 μm (see Table 2).

Table 1 Chemical composition of GGBFS used in RRT1 and RRT2, as determined by X-ray fluorescence (XRF; shown in plain text) or inductively coupled plasma—optical emission spectroscopy (ICP-OES) after total digestion (shown in italics); LOI is the loss of ignition, measured in air at either 950 or 1000 or 1050 °C

Participant	GGBFS chemical compositions (wt. % as oxide)									LOI [%]
	CaO	SiO_2	Al_2O_3	MgO	SO_3	Fe_2O_3	TiO_2	K_2O	Na_2O	
1	*39.51*	*36.61*	*12.30*	*7.39*	*0.68*	*0.63*	*0.00*	*0.48*	*0.36*	1.48
2	41.86	34.55	10.77	9.11	1.22	0.50	0.63	0.35	0.64	–
3	41.92	34.32	9.28	7.71	0.91	0.64	0.71	0.39	0.26	−0.80
4	34.81	37.63	17.92	7.80	0.20	0.66	–	–	–	0.26
5	41.00	34.46	14.40	8.46	2.43	0.22	0.74	0.36	0.54	0.62
6	37.90	43.60	10.70	5.30	1.30	0.20	0.50	0.20	0.00	–
7	54.00	37.50	3.30	1.02	1.95	0.35	0.66	0.39	0.01	0.37

Participants 8, 9 and 10 did not perform chemical characterization of GGBFS

Table 2 Physical properties of GGBFS used in RRT1 and RRT2

Participant	GGBFS source	d_{50} (µm)	BET surface area [cm^2/g]	Blaine fineness [m^2/kg]	Relative density [kg/m^3]
1, 8, 9, 10	EcoCem Benelux B.V. (Ireland)	–	–	395	2910
2		10.21	–	–	–
3		10.47	–	–	3010
7		13.58	2054	–	–
4	ASTRAA chemicals (India)	13.93	–	390	2850
5	Shaoguan steel factory (Guangdong Province, China)	12.84	5948	–	2947
6	NSBFSCem (Japan)	–	–	406	2910

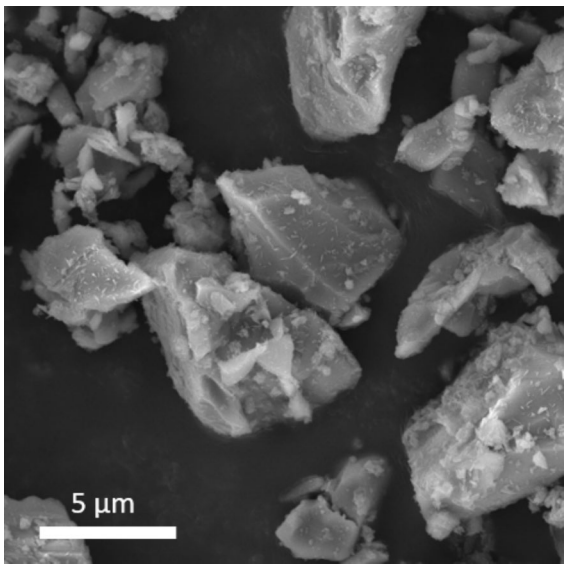

Fig. 1 Morphology of the raw GGBFS powder (SEM image at 10 000 × magnification), obtained by participant 7

2.1.2 Activator

The compositions of the alkali activators (a combination of sodium silicate and sodium hydroxide) used by each participant are listed in Table 3. The activator solution was obtained by combining NaOH pellets (chemically pure) or NaOH solution, deionized water, and sodium silicate solution. The brands or suppliers of the chemicals were not specified, allowing participants to source them based on their local availability (see Table 3) with a target silicate modulus (Ms modulus, SiO_2/Na_2O_{eq}) of 1.03. However, the final compositions of the activators prepared by all participants remained consistent (as described in § 2.2). The detailed activator solution preparation protocol is described in § 2.3.

Table 3 Composition, type, and source of activator solution

Participant	Sodium silicate (Na_2SiO_3) solution [%]				NaOH	
	Source	H_2O	SiO_2	Na_2O	Source	Type
1	PQ Corporation	55.5	29.7	14.8	–	(> 99%) pellets
2		55.0	30.0	15.0	Brenntag N.V	
3		55.0	30.0	15.0	Brenntag N.V	
4		55.9	29.4	14.7	–	
5	Jingcheng Chemical Technology CO	59.6	28.2	12.2	–	
6	Nippon Chemical Industria SS-J1	45.2	37.2	17.6	FUJIFILM Wako Chemicals	
7	Ingessil S.r.l (Italy)	55.7	29.8	14.4	Sigma-Aldrich	
8	Silmaco	18.0	54.5	27.5	–	
9	PQ Corporation	55.0	30.0	15.0	Brenntag N.V	
10	Fisher Scientific	61.7	25.5	12.8	William Clements (Chemicals) Ltd	solution (30%)

Table 4 Type and source of fine and coarse aggregates

Participant	Fine aggregates			Coarse aggregates		
	Type	Size [mm]	Supplier	Type (crushed)	Size [mm]	Supplier
1, 2, 8, 9	river sand	0–4	Coeck (Belgium)	porphyry	4–20	Holcim (Belgium)
3	local sand		Rudus (Finland)	granite		Rudus (Finland)
4	local sand		S.S.B. Enterprises Pvt Ltd, Hyderabad, TS, India	granite		S.S.B. Enterprises Pvt Ltd, Hyderabad, TS, India
5	local sand	0–4.75	-	granite	4.75–20	–
6	crushed sandstone	0–5	Yayoisekizai (Japan)	sandstone	5–20	Yayoisekizai (Japan)
7	river sand	0–4	Concave (Italy)	granite	4–20	Concave (Italy)
10			–	basalt		James Boyd & Sons (Northern Ireland)

2.1.3 Aggregates

Participants 1, 2, 8, and 9 used coarse and fine aggregates from the same suppliers, while the other participants used locally available aggregates. The aggregate properties which comply with EN 12620 [41] and ASTM C33/C33M-18 [42] are summarized in Table 4.

2.2 RRT1 mix design

The objective of the RILEM TC 294-MPA RRT1 expert group was to obtain GGBFS-based AAC with a target consistence class S4 [43] and a target compressive strength class ~ C40/50 [43] at the age of 28 days. The RRT1 trial-and-error interlaboratory investigation comprised of three phases and was performed by participants 1, 2 and 4.

In Phase I, based on previous research conducted by RILEM TC 247-DTA and the latest published findings, the initial mix design of the S3a mix [6] was proposed as the starting point for the exploration of GGBFS-based AAC mix design in the current trial-and-error investigation. Materials available locally at each participant's location were used for AAC production. The initial mix design included 375 kg/m^3 of GGBFS, with a w/s ratio of 0.382, Ms modulus of 0.65 and a target density of 2375 kg/m^3. The obtained results revealed a relatively high compressive strength in the range of 60 to 70 MPa at 28 days with the curing procedure described in §2.3. However, the degree of workability of the mixes did not meet the requirements, since only the consistence class S1 was obtained.

In Phase II, various combinations were explored, with precursor amounts ranging from 420 to 475 kg/m^3, to achieve a desired high workability of the AAC mix. Two mixes, namely S0.45–1 (comprising GGBFS from EcoCem and alluvial gravel) and S0.45–2 (comprising GGBFS from CRH and crushed porphyry from Holcim, Belgium), were evaluated. Both mixes, with a GGBFS amount of 450 kg/m^3, Ms modulus of 0.45, w/s ratio of 0.397, and design density of 2360 kg/m^3, were considered satisfactory. Mix S0.45–1 exhibited a target consistence class S4 with a slightly lower compressive strength (49.6 MPa), whereas mix S0.45–2 demonstrated a slightly higher compressive strength (51.1 MPa) with a medium workability (consistence class S3). For the interlaboratory study, European participants utilized the same batch of GGBFS (EcoCem, Ireland) and aggregates as shown in Table 4, while participants from China, India, and Japan used their own available materials.

In Phase III, mix S.045–2 was replicated using freshly delivered GGBFS (EcoCem, Ireland) and porphyry aggregates by participants 1 and 2. Although the consistence classes ranged from S3 to S5, the compressive strength reached only 37 MPa. To address the issue of low compressive strength, the activator and water content were increased in the mix design, because the activator dose served as a parameter to manipulate the concrete strength. Finally, AAC mix M2 from participant 2, consisting of 450 kg/m^3 of GGBFS, Ms modulus of 1.03, and w/b ratio of

Table 5 Selected RRT1 GGBFS-based AAC (M2) mix design composition requirements

Precursor (GGBFS) [kg/m^3]	450
Na_2O wt. % of GGBFS	4.3
SiO_2 wt.% of GGBFS	4.3
Water wt. % of GGBFS	46
Dry sand (0/4) [kg/m^3]	$626 \le x \le 714$
Dry aggregates (4/20) [kg/m^3]	$956 \le y \le 1072$

0.46 was verified by participants 1 and 4, and it was selected for the interlaboratory study as the RILEM TC 294-MPA RRT1 GGBFS-based AAC (M2) mix (mentioned further in the text as 'RRT1 GGBFS-based AAC (M2)'). The RRT1 M2 AAC mix composition requirements are presented in Table 5. The mix compositions were slightly modified by each participant based on the properties of locally available materials. It is important to highlight that the fine and coarse aggregates used in preparing GGBFS-based AAC mixes were oven-dried at 105℃ to constant weight for 24 h prior mixing.

The selected RRT1 GGBFS-based AAC (M2) mix exhibited a high 28-day-old compressive strength ranging from 54 to 66 MPa and consistence class S4. By this, the RRT1 trial-and-error interlaboratory investigation was concluded in September 2021. The AAC mixing guidelines were developed during the trial-and-error interlaboratory investigation to ensure that all participants strictly adhered to the steps for AAC mixing and curing until the test day, facilitating standardized reporting of their results. The RRT1 GGBFS-based AAC (M2) mix volume was recommended to be followed as 1.0 m^3 by participant 6.

Two additional mixes were involved in the RRT2 tests considering the practical scenario wherein AAC exhibited a reduced workability upon delivery to the site prior to casting. These mixes involved the addition of 5 L and 10 L of extra water per cubic meter of AAC to improve their fresh properties. Specifically, the RRT1 mix and the mixes with additional 5 L and 10 L of water tested in RRT2 were labelled as M2, M2(+5), and M2(+10), respectively.

The RRT1 tests were conducted from September 2021 to March 2024. The RRT2 tests were conducted from October 2021 to July 2023.

2.3 GGBFS-based AAC mixing and curing guidelines

The mixing and curing guidelines underwent a trial-and-error process of interlaboratory investigation aimed at ensuring uniform and high-quality mixing and curing practices across all participants. These guidelines consist of seven sequential steps, as follows:

Step 1. The preparation of the alkali activator initiates 24 h prior to the concrete mixing process to facilitate the complete dissolution of sodium hydroxide pellets. This procedure involves blending solid NaOH with half of the water required for the mix, allowing it to cool to ambient temperature over several hours. The NaOH solution typically achieves ambient temperature within this timeframe. To optimize efficiency, it is advisable to commence preparing a two-part activator at the outset of the day (Part I) and subsequently adding sodium silicate once the solution has adequately cooled by the end of the day (Part II).

- **Part I:** The process commences by dissolving a specified quantity of NaOH pellets in water ("to add") for the mix (if a commercial NaOH solution is available, proceed to Part II). In an available empty plastic bucket or laboratory container, pellets are added first, followed by water. The container is promptly sealed tightly to prevent mass loss. Thorough agitation is applied, and the solution is allowed to cool. Typically, the temperature stabilizes around 60 °C. If prepared the day before, the solution is typically ready for use the following day. To ensure precision, the empty container is weighed, and then re-weighed with NaOH and water solution, followed by another measurement the next day to confirm the accurate total mass of water and NaOH. Immediate sealing after water addition ensures no mass is lost.
- **Part II:** The subsequent day, the prescribed amount of sodium silicate solution is weighed and added to the same container containing the pre-prepared solution of dissolved and cooled NaOH and water. The mixture is then thoroughly combined. A slight temperature increase may occur, and the mixture is allowed to cool to the desired mixing temperature. Typically, the cooling duration for both Part I and Part II in one container ranges between 60 and 90 min at the temperature

of 20 ± 2 °C. However, the actual cooling time is subject to variations based on the laboratory conditions, regional climate, and seasonal factors. It is essential to record relative humidity (RH) and temperature during the mixing process.

Step 2. The AAC mixing process involves combining coarse crushed aggregates (such as porphyry, granite, or basalt), fine aggregates (sand), and precursor materials (GGBFS) in a mixer for approximately 1 min. Concurrently, while the mixer is operational, the activator solution with the rest of the water is gradually introduced into the mixer. The overall mixing duration spans from 3 to 5 min until a workable and homogeneous mass is achieved. Maintaining aggregates under dry conditions is imperative for maintaining reliability in workability and mechanical properties. Empirical observations have demonstrated that the disparity between wet and dry aggregates can yield in a discrepancy in the slump values of up to 10 cm. Moreover, sieving aggregates to eliminate fines or dust is essential.

Step 3. Once the mix is prepared, a slump test is immediately conducted.

Step 4. Following the slump test, the prepared AAC batch is promptly transferred into moulds. To ensure proper compaction, a vibrating or jolting table is employed. The mould is half-filled and vibrated for approximately 10 s, or alternatively, subjected to jolting with one hit per second. The mould is then filled completely and vibrated or jolted for another approximately 10 s. Notably, a significant setting occurs during the casting process, emphasizing the importance of casting of the entire batch within 30 min without a further delay.

Step 5. The freshly produced AAC specimens, once placed in moulds, must be covered on top with a plastic film and wrapped entirely in plastic film from all sides while still in the moulds. These wrapped specimens are stored at a temperature of 20 ± 2 °C and a RH of 55% until the subsequent day. To maintain the RH steady over time, a humidity-controlled chamber can be used, if available.

Step 6. After 24 h, the specimens are demoulded, weighed and immediately tightly sealed in plastic bags to prevent air exposure. It must be noted that if hardening problems are observed after 24 h, it is advisable to demould specimens after 48 h. If a vacuum sealer machine is accessible, it presents an optimal solution for airtight sealing. The sealed samples should be then stored at the temperature 20 ± 2 °C until the testing day. Alternatively, applying Vaseline on the AAC specimens' surface and subsequently sealing them airtight with plastic film is an alternative approach, as depicted in Fig. 2.

Step 7. On the testing day, the specimens are weighted and measured to record their densities and any mass loss over the specified period.

2.4 Testing methodology

All participants were directed to leverage established expertise, facilities, and the detailed guidelines to produce AAC in accordance with the

Fig. 2 Sealing of the specimens after demoulding until any test (photo taken by participant 2)

developed mix design of the RILEM TC 294-MPA RRT1. In the absence of testing procedures for AAC within the existing EN and ASTM standards, the participants independently adapted standard test methods to align with their respective facilities. Each participant, equipped with substantial expertise in both the production and testing of AAC, deployed personnel, including technical staff, (post-)doctoral researchers, or seasoned graduate students—to execute the agreed-upon RRT1 GGBFS-based AAC mixing and casting procedures. Given the limited availability of the testing equipment, the participants conducted tests based on the resources available at their respective facilities.

2.4.1 *Slump, flow and rheology tests*

The concrete slump test was performed according to EN 12350-2 [44] or ASTM C 143 [45]. RRT2 tests were performed periodically, extending up to 2 h after the first measurement, to assess the workability retention of AAC. Specifically, slump tests were performed immediately after the GGBFS-based AAC mix was produced (approximately 5 min after wetting the precursor), and then repeated at intervals of 30, 60, and 120 min.

The concrete flow test was performed according to EN 12350-5 [46] or ASTM C1621 [47]. The AAC mix underwent a 60 s remixing process using a mixer after conducting slump and flow table tests at 30-, 60-, and 120-min intervals. Each mix composition underwent three test replications, and the resultant average values were recorded for the slump and flow diameter assessments. It is crucial to acknowledge that the participants used different types and sizes of mixers, which could have influenced the measured results. Additionally, variations in laboratory conditions, such as temperature and RH may have affected the fresh properties of the GGBFS-based AAC mix. The details of the test conditions are listed in Table 6.

The rheological behaviour was evaluated using an ICAR Plus rheometer to characterize the static yield stress, the dynamic yield stress, and plastic viscosity of GGBFS-based AAC [48]. A detailed description of the procedure is provided in Appendix 1.

2.4.2 *Density*

The density of AAC can be determined according to EN 12390-7 [49] or ASTM C138/C138M [50] standards. Three replicate cube or cylinder specimens were tested to determine the average density for each age. Upon demoulding, the cast specimens were immediately covered with a plastic wrap until testing to mitigate excessive moisture loss.

2.4.3 *Compressive strength*

The compressive strength tests were conducted on cubes with dimensions of 100 mm × 100 mm × 100 mm or 150 mm × 150 mm × 150 mm and cylinders with dimensions of 100 mm × 200 mm or 150 mm × 300 mm at ages of 1, 3, 7, 28, 90, 180, 360, and 720 days in accordance with EN 12390-3 [51] or ASTM C39/C39M-21 [52]. In cases, where cylindrical specimens were used under either protocol, the results were multiplied by a factor of 1.25 to convert to equivalent cube strengths, allowing an equivalency in strength classes in EN 206 [6, 43]. A reduction factor of 0.95 for compressive strength

Table 6 Testing conditions reported by different participants in RRT2

Participant	Mixer	Testing temperature (°C)
2	Drum mixer by gravity	20 ± 1.0
3	Planetary mixer	22.9
4	Industry grade drum rotary mixer	31 ± 2.0
9	Gustav Eirich SKG1 planetary mixer	16 ± 1.0
10	Croker Cumflow RP50XD rotating pan mixer	20 ± 1.5

was applied to cube specimens with dimensions of 100 mm × 100 mm × 100 mm [53]. Three replicate cube or cylindrical specimens were tested to determine the average compressive strength values for each age. Upon demoulding, the specimens were immediately covered with plastic wrap until testing to prevent excessive moisture loss.

2.4.4 Splitting tensile strength

The standardized splitting tensile strength tests were performed on 100 mm × 200 mm or 150 mm × 300 mm cylinders at the ages of 1, 3, 7, 28, 90, 180, 360, and 720 days in accordance with EN 12390-6 [23] or ASTM C496/C496-M-17 [24]. Three replicate cylindrical specimens were tested to determine the average splitting tensile strength values for each age. Upon demoulding, the cast specimens were immediately covered with plastic wrap until testing to mitigate excessive moisture loss.

3 Results and discussion

The RRT1 expert group's work included experimental results from eight participants (1 to 8), primarily focused on the mechanical properties of hardened GGBFS-based AAC, such as density, compressive strength, splitting tensile strength, and elastic modulus. The RRT2 expert group's work, based on obtained data from five participants (2, 3, 4, 9 and 10), focused mainly on fresh properties of GGBFS-based AAC, including slump, flow, and rheology. Participants 2 and 4 performed slump tests twice, as they took part in both RRT1 and RRT2 experimental campaigns. All ten participants perform a slump test of RRT1 GGBFS-based AAC (M2) mix within 5 min after casting GGBFS-based AAC. Due to limited availability of testing equipment, rheology and elastic modulus experiments were conducted on a smaller scale, and the obtained experimental data is summarized in Appendices 1 and 2 of this report.

3.1 Slump

3.1.1 RRT1

The slump test results obtained by participants 1 to 8 for RRT1 to verify a target consistence class S4 of GGBFS-based AAC are shown in Figs. 3 and 4.

Participants 1, 2, 3, 4, 5, and 8 successfully attained the target consistence class S4, whereas participants 6 and 7 did not achieve the required

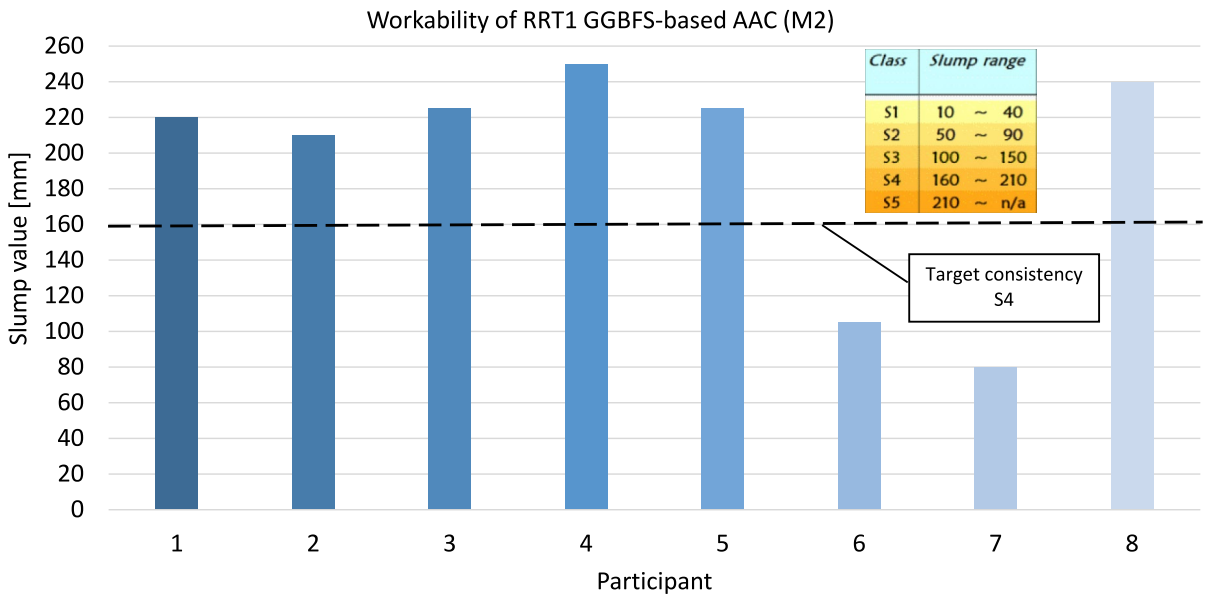

Fig. 3 Slump test results

Fig. 4 Slump test performed by participants 1 to 8

level and obtained a medium workability. This disparity can be attributed to the timing of the slump test, as delayed testing impacted the results. Another reason for the lower slump test values observed by participant 6 could be the different type of aggregates used (see Table 4).

3.1.2 RRT2

The results of the slump tests conducted by participants 2, 3, 4, 9 and 10 in RRT2 are summarized in Fig. 5. As shown in Fig. 5a, almost all participants successfully achieved the target consistence class S4 (i.e., slump > 160 mm) within 5 min as outlined in RRT1. The most significant increase in the slump loss occurred between 5 and 30 min for all participants (Fig. 5b), indicating a high level of early reactivity in the alkali-activated slag system. Subsequently, the slump values declined slightly over time in the subsequent tests. Participant 4 reported a higher slump loss rate over time compared to other participants, possibly due to the use of a drum mixer. Unlike other mechanical mixers, the drum mixer primarily relies on gravity and may not effectively break down an early structuration during remixing, leading to increased slump loss. It is noteworthy that the consistency of GGBFS-based AAC reported by participant 9 reached class S5 within 5 min, with a comparatively lower slump loss than other participants. This might be ascribed to the lower testing temperatures as indicated in Table 6, which could decelerate the early-stage reactions in AAC. Participants 2 and 9 observed considerable increases in slump values accompanied by a lower slump loss over time in M2(+5) and M2(+10), which had a higher water content (Fig. 5c–f). This can be attributed to the dilution of the pore solution, resulting in reduced alkalinity and decreased contribution to the early reaction. However, participant 4 noted that these effects were less significant due to an elevated testing temperature of approximately 31 °C compared to other participants' testing temperatures. Participant 3 observed that waiting for 10 min after casting to perform the slump test resulted in a decrease of up to 97 mm. However, performing the test after only 4 min yielded a significantly different value of 225 mm for the same mix design.

3.1.3 Flowability

The results of the flow table tests are shown in Fig. 6. The largest flow diameter at 5 min was reported by participant 9, exceeding 600 mm, as indicated in Fig. 6a. In general, the flow diameter of the GGBFS-based AAC followed a similar trend to the slump

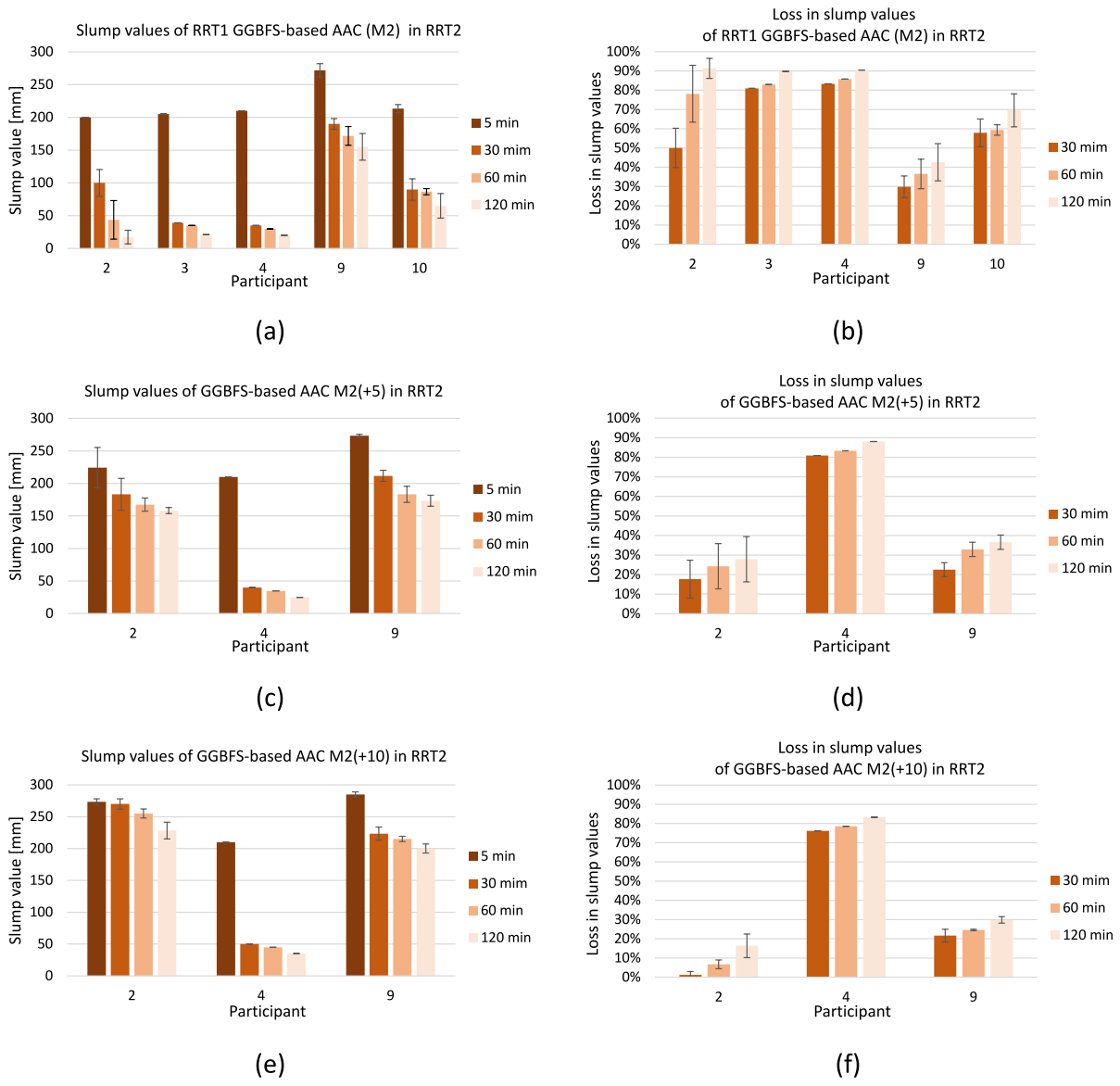

Fig. 5 Slump test results obtained by RRT2

values, deteriorating over time. However, the loss in flow diameters (Fig. 6b) was much less pronounced compared to slump values, likely due to the structural breakdown caused by the shear energy induced by the oscillation of the flow table. Participant 3 observed smaller flow diameters and higher losses, possibly due to a slight increase in temperature. Moreover, the flow diameter gradually increased with the addition of extra water content (Figs. 6c, e), approaching its maximum with 10 L of additional water in the GGBFS-based AAC. Furthermore, as shown in Fig. 6f, the loss in flow diameter was hardly detected, as reported by participant 2, suggesting good workability retention within the first 2 h.

In addition, along with the slump and flow table test results presented in this report, rheological assessments of the RRT1 GGBFS-based AAC (M2) mix in terms of stress growth and flow curve tests were also suggested in RRT2. However, the execution of rheological tests was exclusively undertaken

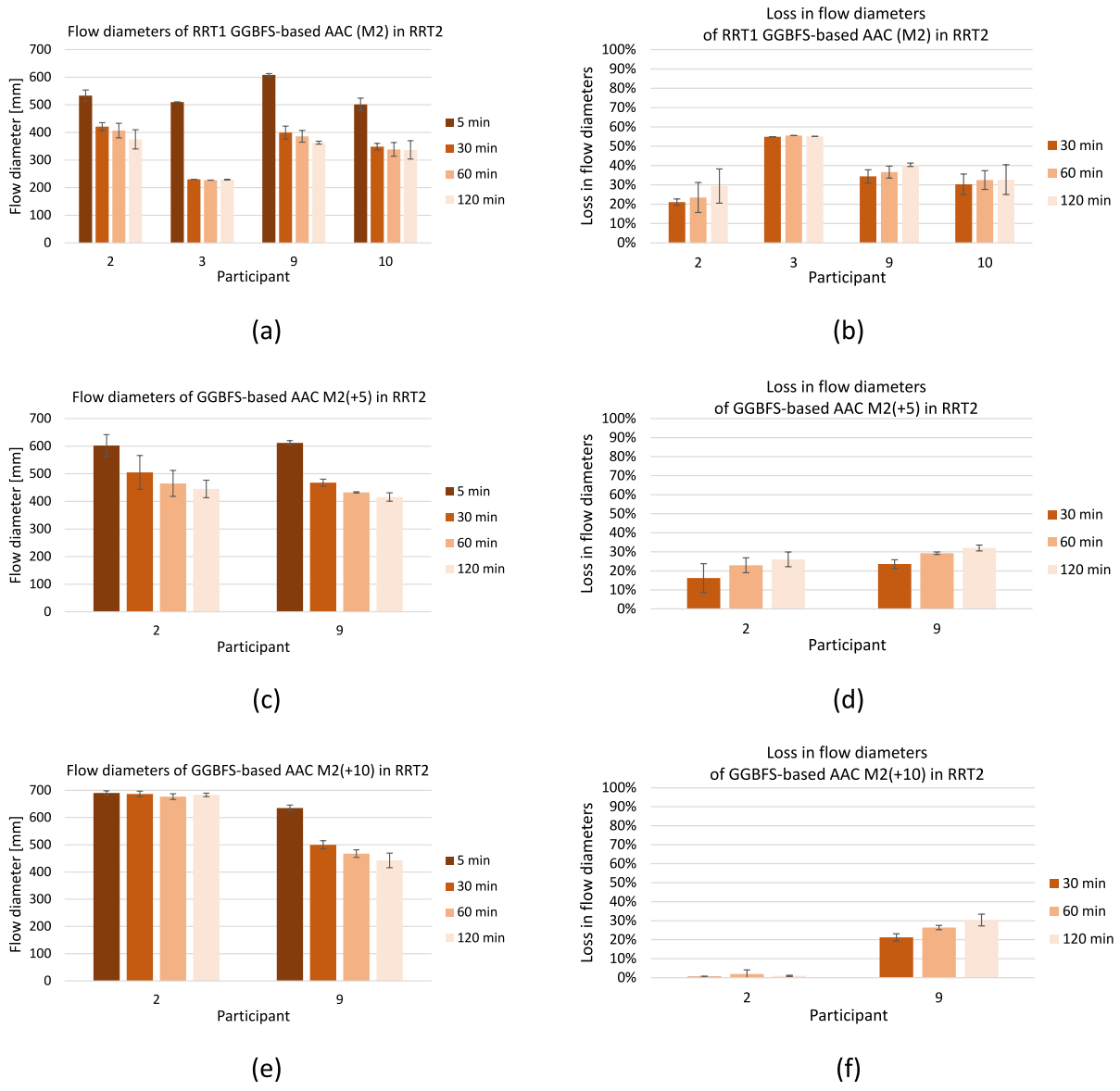

Fig. 6 Flow table test results in RRT2

by participant 9, due to limited availability of testing equipment. Hence, no interlaboratory comparison of the experimental data is possible. The outcome on the rheology of the GGBFS-based AAC mixes – M2, M2(+5) and M2(+10) – is provided for readers in the Appendix 1.

3.2 Densities of hardened GGBFS-based AAC specimens

The density results of the RRT1 GGBFS-based AAC (M2) are shown in Fig. 7. It is apparent that the variation in density from minimum to maximum among all participants fell within the range of 2337–2398 kg/m^3 for 1 day-old specimens, 2333–2385 kg/m^3 for 28 day-old specimens, and 2327–2380 kg/m^3 for 720 day-old specimens.

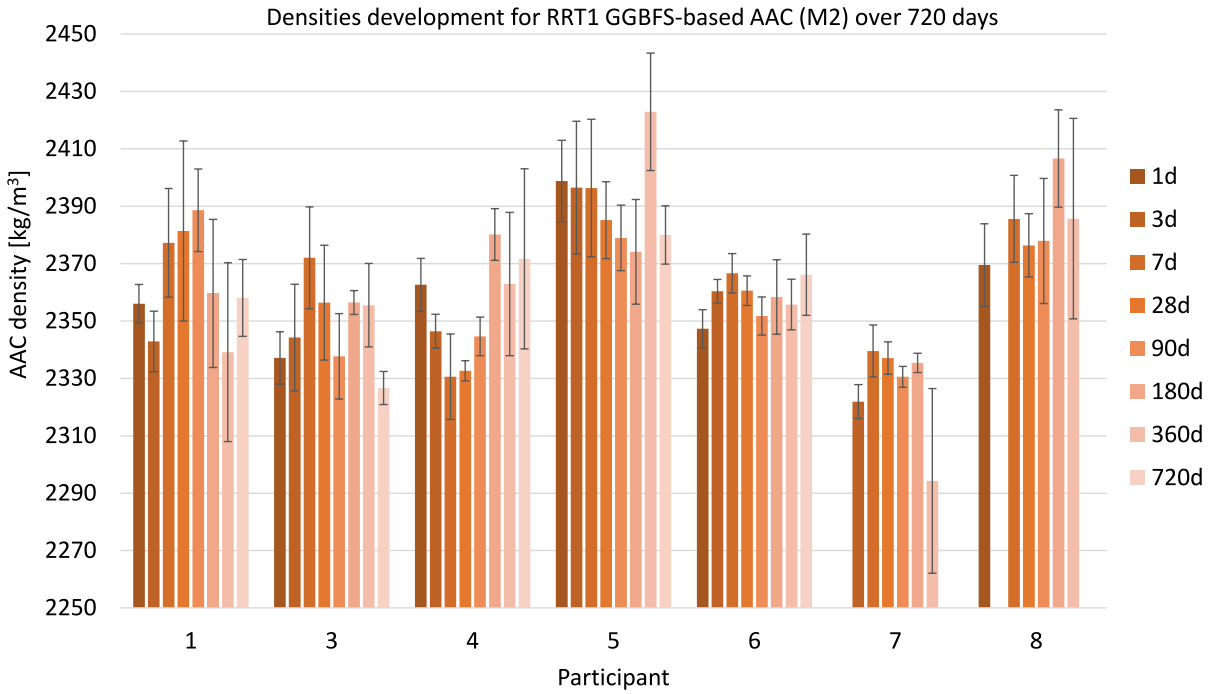

Fig. 7 Densities of hardened RRT1 GGBFS-based AAC (M2)

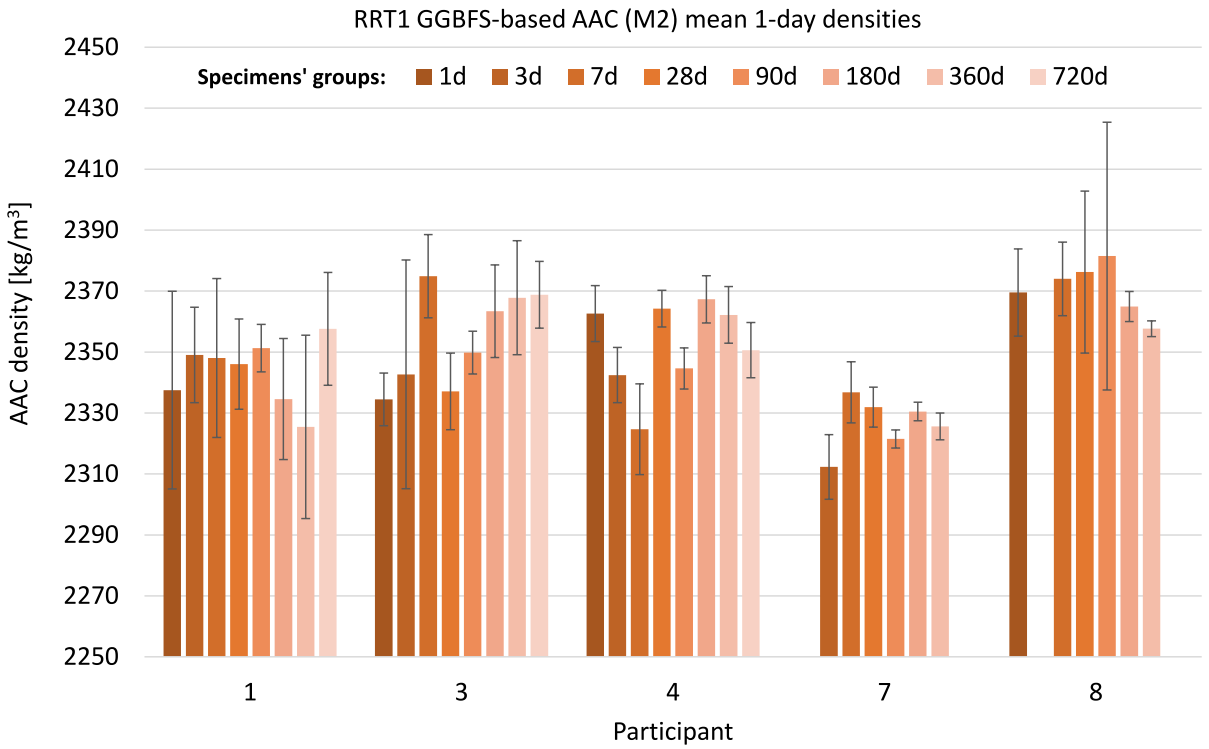

Fig. 8 Mean densities of hardened RRT1 GGBFS-based AAC (M2) specimens at 1-day

This corresponds to a density reduction of 0.1% at 28 days and 0.2% at 720 days. Figure 8 presents the initial average densities of the specimens produced for RRT1 by each participant, with three specimens tested per age group category (e.g., 1d, 3d, …, 720d). All RRT1 specimens were measured for the 1-day density among the participants. Overall, Fig. 8 highlights the variation in density across all specimens from the RRT1 testing campaign.

A noticeable variance in the standard deviations of density was observed across all specimens' groups at different ages. This variance can largely be attributed to delayed casting or improper vibration, resulting in difficulty in placing still-fluid GGBFS-based AAC. As mentioned by Mavroulidou et al. [54], the casting performed by users who were assigned to replicate the authors' tests but did not follow a proper mixing during the experiment, resulted in AAC mixes with notably poor outcomes. To mitigate issues related to delayed manual casting, the production of large batches (> 50 L per batch) was avoided. It is known that this activation can lead to setting times as short as 15 min [55], resulting in challenges during GGBFS-based AAC casting. The specimens were typically demoulded after one day without a damage, emphasizing the importance of maintaining a GGBFS-based AAC mix design volume of 1.0 m^3. No consistent pattern was observed in the density changes among the specimens with age. However, proper sealing and curing can mitigate these potential issues. In addition, depending on the strength development of each specimen over time and various other factors, the density standard deviations either decreased or increased for the same group of three specimens per age category.

3.3 Compressive strength

The compressive strength test results are shown in Fig. 9. All participants reached the target bottom line of 50 MPa for the compressive strength at 28 days. Participant 1 consistently exhibited steady increase in compressive strengths, ranging from 18.5 MPa at 1 day to 55.3 MPa at 28 days and 64.7 MPa at 720 days. Participant 2 showcased higher initial strengths, reaching 31.0 MPa at 1 day, 64.6 at 28 days and concluding with 69.9 MPa at 90 days. Participant 3 reported strengths comparable to participant 1, with values ranging from 17.4 MPa at 1 day to 51.3 MPa at 28 days and 48.3 MPa at 720 days. However, a considerable decrease in compressive strength

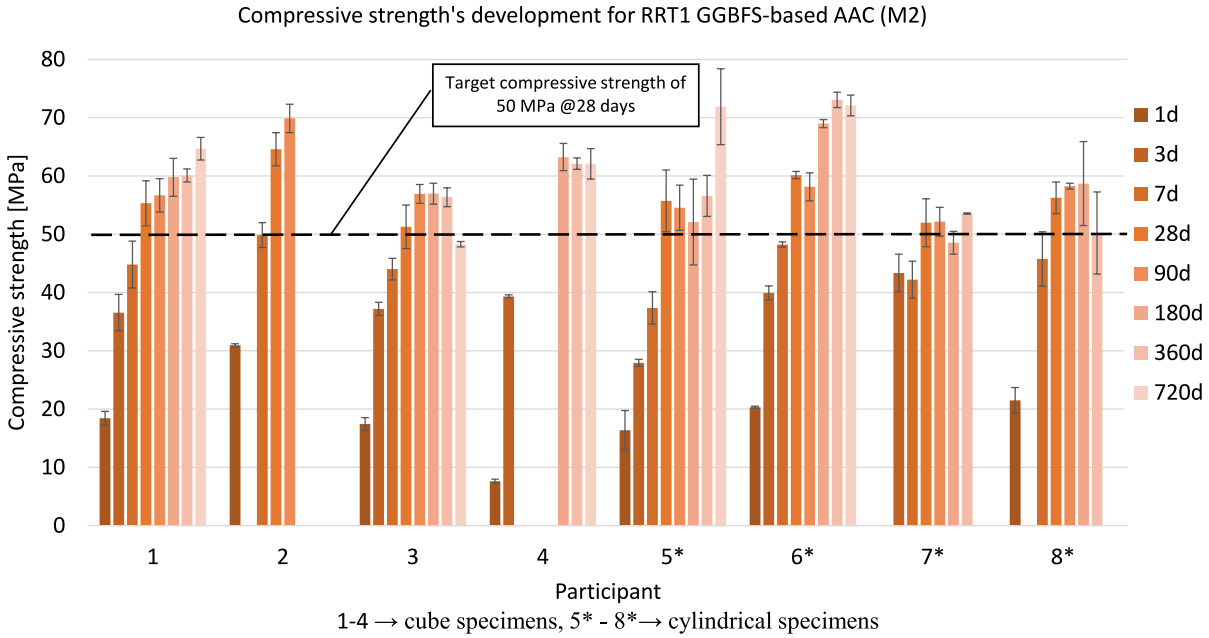

Fig. 9 Compressive strength results for RRT1 GGBFS-based AAC (M2) (note: the values are converted according to §2.4.3)

was identified after 360 days, possibly related to some technical issues during the measurement. Participant 4 showed competitive performance at later ages, spanning from 7.6 MPa at 1 day to 63.2 MPa at 180 days and stabilized there until 720 days. Participant 5 observed competitive strengths ranging from 16.4 MPa at 1 day to 55.7 MPa at 28 days and 71.9 MPa at 720 days. Participant 6 consistently reported higher strengths across all durations, ranging from 20.3 MPa at 1 day to 60.2 MPa at 28 days and 72.1 MPa at 720 days. Meanwhile, participant 7 demonstrated varying strengths, with initial strengths of 43.3 MPa at 3 days increased to 52 MPa at 28 days and remained steady at 53.6 MPa at 360 days. Participant 8 also exhibited variations, with compressive strength reaching 21.5 MPa at 1 day, 56.3 MPa at 28 days, and 50.2 MPa at 360 days. Noting the error bars in Fig. 9, the apparent decrease in the compressive strength was not statistically significant. Participant 7 recorded lower results compared to the other participants, most likely encountering challenges with the mixing procedure or during curing.

The Na_2O and SiO_2 contents in the GGBFS were consistent across all participants, ensuring a standardized composition of the alkali activator (see Table 5). However, variations in alkali activator concentrations, aggregate properties, aggregate moisture conditions, mixing by different operators, and the type of mixer were key factors contributing to differences in compressive strength among participants. Although the participants maintained a consistent w/b of 0.46 across their mix designs, ensuring similar water availability for hydration reactions, applying dried aggregates, variations in sodium silicate solution, and NaOH dosage affected the rate and extent of alkaline activation, and subsequently impacted compressive strength, particularly, for participant 8. Differences in the coarse aggregate types (porphyry, granite, and basalt) also influenced the mechanical properties.

Overall, the variation in results among the eight participants was not significantly greater than the ones reported for PCC [56] and was notably smaller than that observed in the previous AAC studies in the RILEM TC 247-DTA [6]. These findings demonstrate good repeatability and highlight the reliability of the interlaboratory study for the GGBFS-based AAC.

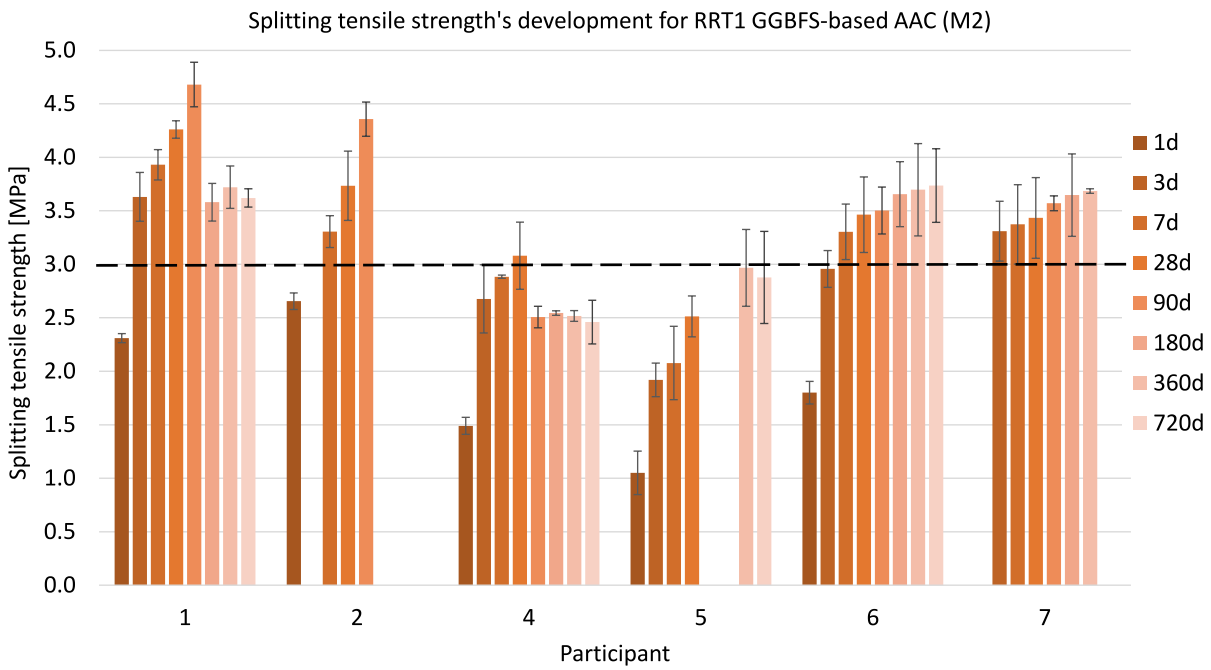

Fig. 10 Splitting tensile strength test results for RRT1 GGBFS-based AAC (M2)

3.4 Splitting tensile strength

The splitting tensile strength test results are presented in Fig. 10.

Participant 1 showcases a gradual increase in splitting tensile strength from 1 to 90 days, with values ranging from 2.3 to 4.7 MPa. The splitting tensile strength obtained by participant 2 reached a similar value of 4.4 MPa at 90 days. Conversely, participant 4 demonstrated splitting tensile strengths ranging from 1.5 to 2.5 MPa across various durations. Participant 5 demonstrated splitting tensile strengths ranging from 1.1 to 3.0 MPa, with missing data for certain durations. Participant 6 reported consistent splitting tensile strengths ranging from 1.8 to 3.7 MPa over the same period, showing stability across different curing periods. Meanwhile, participant 7 exhibited splitting tensile strengths ranging from 3.3 to 3.7 MPa, with a steady increase observed over time.

Variations in splitting tensile strength were evident across participants, with participants 1, 2, 4, 6, and 7 showing consistent performance trends. Participant 1 exhibited a similar strength development tendency as participant 4, although with higher values. Participant 1 observed a decrease in splitting tensile strength from 90 to 720 days. This could be attributed to changes in the curing conditions at the temperatures between 10 and 20 °C. The results for participant 4 may be related to GGBFS-based AAC having a less dense gel matrix with more microcracks or variation in curing practices, or the switch to newer testing equipment during the ongoing interlaboratory study. Participant 2 demonstrated the highest 1-day initial splitting tensile strength, which is in line with their compressive strength results (see Fig. 9). Participant 5 exhibited the lowest initial strengths, while participant 6 consistently reported higher splitting tensile strengths across all durations. Participants 6 and 7 exhibited similar splitting tensile strength development tendencies. Participant 7 displayed a moderate splitting tensile strength over all testing periods. Participant 8 did not perform splitting tensile strength tests.

The analysis of the splitting tensile strength data revealed varying performance trends among the participants. While participants 1, 2, 4, 5, 6, and 7 exhibited a gradual increase in splitting tensile strength with curing duration until 28 days, a coherent evaluation of the decrease or increase after 90 days could not be performed due to limited experimental data from all participants. Variations in the curing temperatures and environmental conditions across different regions where the participants were situated could have impacted on the hydration kinetics and mechanical properties of the GGBFS-based AAC specimens. Nevertheless, the bottom line of the splitting tensile strength is 3 MPa in RRT1.

3.5 Non-linear relationship between the compressive and splitting tensile strengths

Based on the provided data, there is a correlation between the compressive and splitting tensile strengths of the GGBFS-based AAC specimens tested across different participants and curing durations. The correlation suggests that as the compressive strength increases, the splitting tensile strength tends to increase, and vice versa, with similar strength development tendencies. This suggests that factors influencing the compressive strength, such as the GGBFS-based AAC mix design, curing conditions, and aggregate properties, also have an impact on the splitting tensile strength.

The power model was fitted to the experimental data to establish a predictive relationship between 28-day compressive strength (f'_c) and splitting tensile strength ($f_{ct,sp}$). Using R software, a non-linear regression analysis was conducted with the model (Eq. 1) defined as:

$$f_{ct,sp} = a \cdot (f'_c)^b \tag{1}$$

The regression analysis yielded the optimized parameter values a = 0.0241 and b = 1.2056. The proposed model (Eq. 2) is as follows:

$$f_{ct,sp} = 0.0241 \cdot (f'_c)^{1.2056} \tag{2}$$

Table 7 Non-linear regression metrics

Parameter	Value
MAE	0.12
RMSE	0.15
R^2	0.94

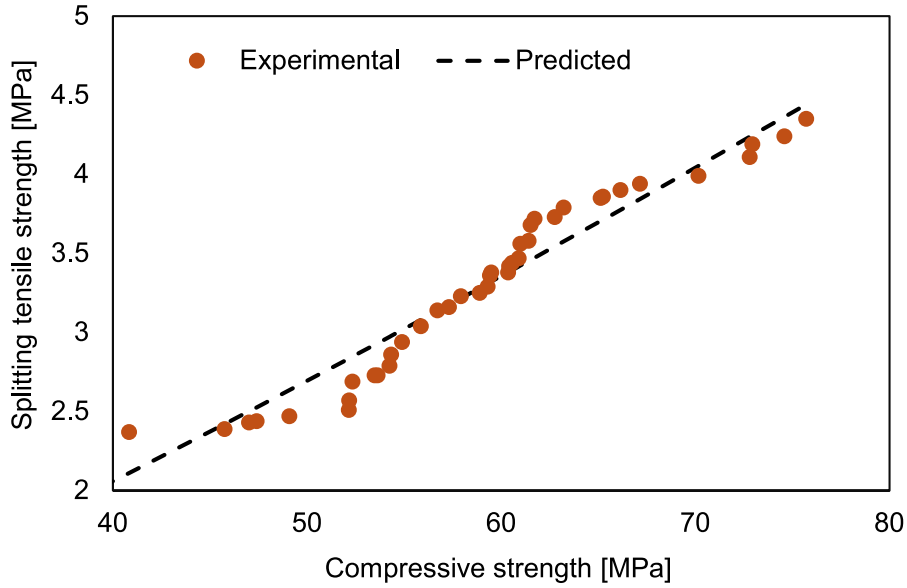

Fig. 11 Experimental vs predicted relation between compressive and splitting tensile strengths for RRT1 GGBFS-based AAC (M2)

The results from the non-linear regression analysis are presented in Table 7.

The R^2 value for this model was calculated as 0.94, indicating a strong fit between the predicted splitting tensile strengths and the observed data. This high R^2 value suggests that the power model effectively captures the underlying trend in the data, highlighting its suitability for representing the relationship between compressive and splitting tensile strengths in cementitious materials. The model's performance was further examined by plotting the fitted curve against the observed values. Figure 11 shows the compressive strength versus splitting tensile strength data points alongside the model's predicted curve, demonstrating close alignment between the observed data and model predictions, particularly at mid-to-high compressive strengths.

The power model was chosen for its ability to capture non-linear relationships, which are commonly observed between compressive and splitting tensile strengths in cement composites. The exponent b, estimated at 1.2056, suggests a super-linear increase in splitting tensile strength relative to compressive strength.

The high R^2 value (0.94) confirms the model's effectiveness in predicting splitting tensile strength across a range of compressive strength values. This is particularly beneficial in practical applications where splitting tensile strength measurements are needed but challenging to obtain directly. The power model thus provides a reliable empirical method for estimating splitting tensile strength from more accessible compressive strength data.

However, the model's accuracy diminishes slightly at lower compressive strength values, as indicated by minor deviations from the observed data in this range. This limitation suggests that the power model performs best when applied to AAC with moderate to high compressive strengths. For lower-strength AAC, alternative models or additional data points may be required to enhance predictive accuracy.

In conclusion, the power model, implemented using R software, offers a robust and practical approach for estimating splitting tensile strength from compressive strength. Future research could explore modifications to this model to improve predictions for low-compressive-strength AAC.

4 Summary and conclusions

This report introduced globally reproducible GGBFS-based AAC mix design and mixing guidelines based on a trial-and-error interlaboratory investigation followed by the interlaboratory study among the participants of the RILEM Technical Committee 294-MPA. Ten participants from Belgium, China, Finland, India, Italy, Japan, the Netherlands, and the United Kingdom took part in the testing campaign.

Although alkali-activated materials have been recognized for nearly a century, there is limited knowledge and experience in their use to produce AAC in the construction sector. It is mostly related to the absence of standards and a straightforward production flowsheet due to the variability in material composition, mixing techniques, and casting procedure of AAC. The mechanical and fresh properties of GGBFS-based AAC are primarily influenced by the mix proportions. The complexity of AAC mix design arises from the manifold variables that impact the alkali-activation process, including alkali content, curing parameters (time, relative humidity and temperature), water-to-solid ratio, pH, activator molarity, raw material composition and type, activator, and silicate-to-hydroxide ratio. The recent four-year experimental campaign conducted by RRT1 and RRT2 expert groups generated valuable first-hand data on the properties of fresh and hardened AAC. These data enhance the understanding of AAC characteristics and repeatability of related experiments. The insights presented in this report could support efforts towards the standardization of AAC.

The main findings can be summarized as follows:

- A structured mix design experimental campaign and GGBFS-based AAC mixing and curing guidelines were developed, enabling participants to replicate the mix with good reproducibility across different settings and local material availability.
- Nearly all participants met the initial target consistence class S4 and achieved the required compressive strength threshold of approximately 50 MPa at 28 days.
- The RRT1 results indicated that across all participants, the average compressive strength values reached 56 MPa at 28 days and 64 MPa at 720 days. The average splitting tensile strength, observed over the 720-day period, stabilized at 3.2 MPa. Notably, the observed interlaboratory deviations were largely aligned with the expectations for the PCC.
- The RRT2 results indicated that all participants achieved consistence class S4 within 5 min after casting GGBFS-based AAC, followed by a rapid slump loss, confirming the well-known reaction rate in the alkali-activated slag system. The flow diameter of AAC followed a similar trend to the slump test values, although with a less noticeable loss over time. The largest flow diameter, measured at 5 min, surpassed 600 mm. Some smaller flow diameters and higher reductions were observed, potentially due to a slight increase in temperature. It was noted that both the types of mixing equipment and lab temperature can affect the slump loss. Remarkably, the addition of extra water to the GGBFS-based AAC mix resulted in higher initial slump test values, reduced slump loss over time, and a progressive increase in flow diameter, reaching its peak with 10 L of added water. This suggests an effective practical approach for adjusting the workability of GGBFS-based AAC. However, it is important to note that strength and durability may decrease with an increase in water amount, so this should be considered during the adjustment of workability.

Acknowledgements The authors thank Dr. Dong Hua (TU Delft, The Netherlands), Mr. Hu Shi (TU Delft, The Netherlands), Mr. Chen Liu (TU Delft, The Netherlands), Ms. Elisa Wirkkala (University of Oulu, Finland), Ms. Pujitha Ganapathi Chottemada (BITS, India), Ms. Liu Zhang (Guangzhou University, China), Mr. Xiaocong Yang (Guangzhou University, China), Mr. Chongxi Yang (Guangzhou University, China), Eng. Francesca Ballestrazzi (University of Bologna, Italy), Eng. Giorgio Virgulto (University of Bologna, Italy), Prof. Maria Chiara Bignozzi (University of Bologna, Italy), Prof. Claudio Mazzotti (University of Bologna, Italy), Mr. Abdo Shamseldin (SCK CEN, Belgium), Mr. Mukiza Emile (SCK CEN, Belgium), Mr. Xiaodi Dai (Ghent University, Belgium), Ms. Beibei Sun (Ghent University, Belgium) and Dr. Meng Gao (Queen's University Belfast, United Kingdom) for their help with the experiments. The authors thank EcoCem Benelux B.V. (Ireland) for providing GGBFS for European RRT1 and RRT2 participants; Dr. Arno Keulen (CRH) for providing GGBFS for the RRT1 interlaboratory trial-and-error experimental investigation; Mr. Pieter Ballie (Holcim (Belgium)) for providing porphyry aggregates for the Belgian and Dutch RRT1 and RRT2 participants. The authors would also like to thank their respective institutes, organizations and companies for providing the resources necessary to prepare this study.

Author contributions All authors contributed to the study. All authors have read and approved the final manuscript. Writing—original draft preparation: Patricia Kara De Maeijer, Kruthi Kiran Ramagiri and Yubo Sun. Writing—review and editing: Juho Yliniemi, Zhenming Li, Guang Ye, Quoc Tri Phung, Wei Sha, Yubo Sun, Kruthi Kiran Ramagiri and Patricia Kara De Maeijer. Writing—review: Giulia Masi, Kazuo Ichimiya, Arkamitra Kar, Yuwei Ma, Frank Dehn and Geert De Schutter.

Declarations

Conflict of interest This paper was prepared through the joint and collegial efforts of the RRT1 and RRT2 Expert groups from the RILEM Technical Committee 294-MPA. The authors have no conflicts of interest to declare that are relevant to the content of this paper. The RRT1 and RRT2 results provided by participants are meant for the publication in the Journal of Materials and Structures as RILEM TC Report.

Appendix 1

Rheology assessment on GGBFS-based AAC

The rheology assessments on GGBFS-based AAC testing were exclusively carried out by participant 9. It comprised of stress growth and flow curve steps, were performed on three GGBFS-based AAC mixes (M2, M2(+5), and M2(+10)), as outlined in RRT2, using an ICAR Plus rheometer featuring a coaxial cylinder geometry. Initially, approximately 20 L of fresh batch of GGBFS-based AAC were loaded into a cylindrical rheometer container with a depth of 390 mm and an inner diameter of 286 mm. Prior to each set of tests, the GGBFS-based AAC within the rheometer container underwent a preliminary remixing process using a handheld mixer for 60 s. This step was implemented to eliminate any thixotropic build-up and ensure uniformity of the reference state across different specimens. Subsequently, a rheometer vane, characterized by four blades with dimensions of 130 mm in diameter and 130 mm in height, was inserted. Following this, the fresh GGBFS-based AAC was allowed to rest for approximately 1 min to dissipate any residual energy accumulated from the conclusion of the remixing process until the commencement of the rheological test.

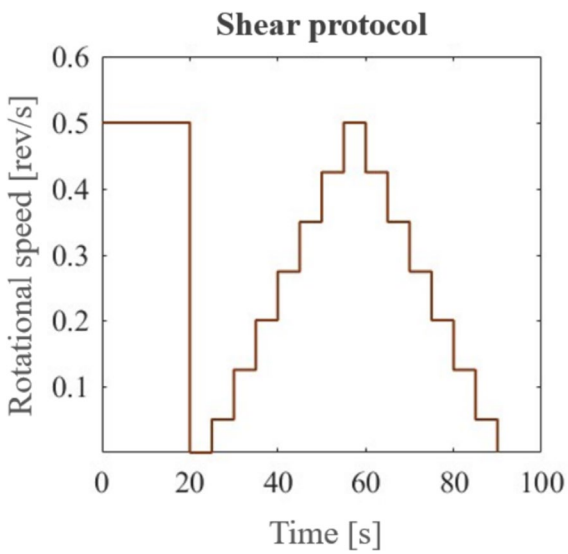

Fig. 12 Shear protocol used for the flow curve tests

The stress growth test was initiated 10 min after the precursors were wetted. A constant rotational speed of 0.025 revolutions per second (rev/s) was applied for 60 s, during which the maximum observed torque was converted into a static yield stress using the methodology of Koehler and Fowler [57]. Subsequently, flow curve tests were conducted on the same batch of GGBFS-based AAC following the protocol shown in Fig. 12. Initially, the fresh batch underwent a 20-s pre-shear at 0.5 rev/s, followed by sequential ascending and descending shear steps. The rotational speed ranged from 0.05 to 0.5 rev/s with increments of 0.05 rev/s, with each step lasting 5 s to determine the average torque value. Bingham linear fitting was applied to the descending segments of the torque-rotational speed relationship to derive the flow curves. The dynamic rheological parameters of the GGBFS-based AAC were determined using the Reiner-Riwlin equations [58]. For each GGBFS-based AAC mix composition, the rheological parameters were determined as the average of tests conducted on three replicate specimens.

The rheological characteristics of GGBFS-based AAC, as assessed by participant 9, are presented in Fig. 13. Notably, the highest static yield stress was detected in the reference mix RRT1 GGBFS-based AAC (M2), as shown in Fig. 13a. It was found that the static yield stress of GGBFS-based AAC decreased by 12% and 27% with addition of 5 and 10 L of extra water, respectively. These findings suggest that increasing the water content has a mitigating effect on the early structuration, necessitating less shear energy to initiate the flow of GGBFS-based AAC from a static state. Moreover, the ramp-down flow curves, as presented in Fig. 13b, along with the dynamic yield stress and plastic viscosity derived from the Bingham linear fitting, are shown in Figs. 13 c and d, respectively. In line with the results obtained from the stress growth tests, a gradual decline in dynamic rheological parameters was observed with increasing water content. This underscores the dispersing effect of water

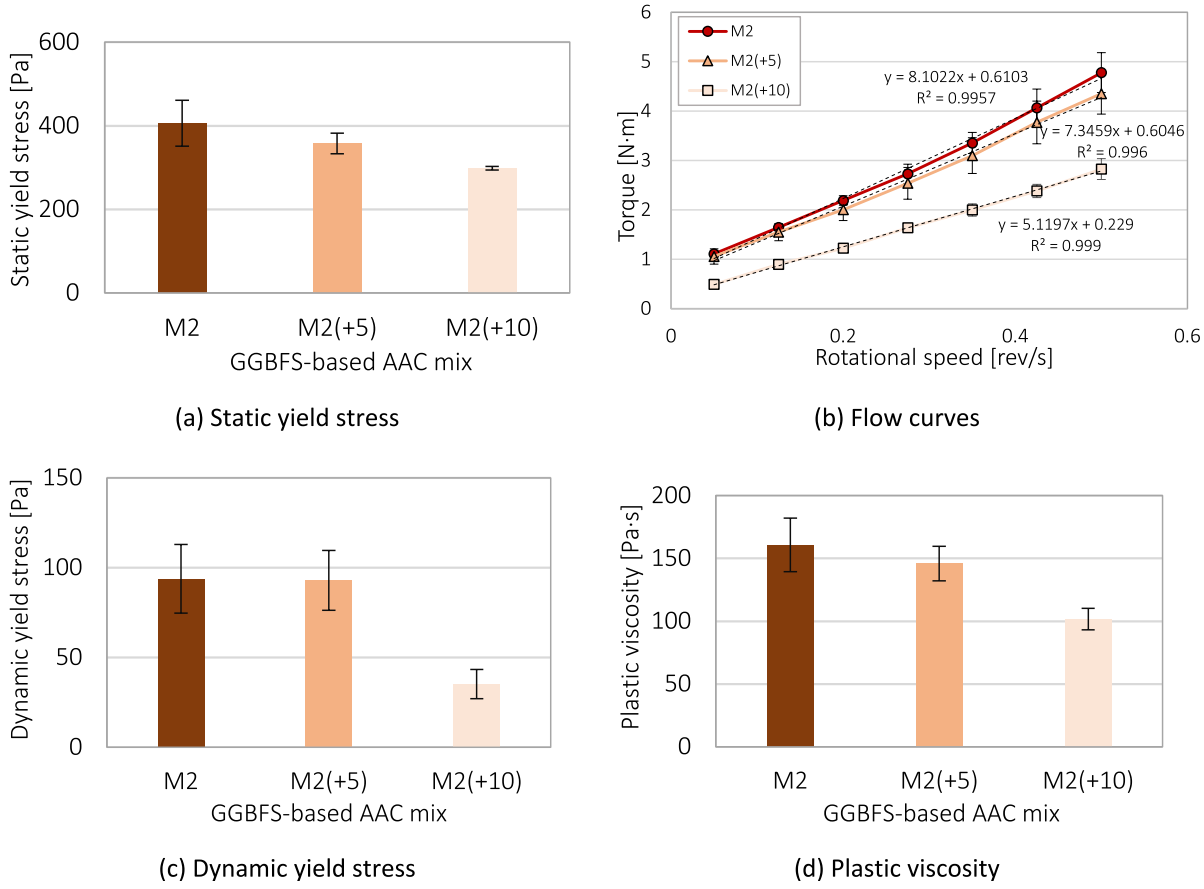

Fig. 13 Results of rheological tests

in the GGBFS-based AAC, resulting in reduced shear energy requirements to sustain steady dynamic flow. In comparison to the reference mix RRT1 GGBFS-based AAC (M2), the plastic viscosity of GGBFS-based AAC M2(+5) and M2(+10) decreased by 10% and 58%, respectively, with an increase in water content. In general, the rheological performance exhibited a significant enhancement with the addition of extra water, suggesting an effective practical approach to adjust the workability of GGBFS-based AAC.

Appendix 2

Elastic modulus of GGBFS-based AAC

The standardized elastic modulus tests were performed on 100 mm × 200 mm or 150 mm × 300 mm cylinders at the ages of 1, 3, 7, 28, 90, 180, 360, and 720 days in accordance with EN 12390-13 [59] or ASTM C469 / C469M [60]. Three replicate cylindrical specimens were tested to determine the average elastic modulus values for each age. Upon demoulding, the cast specimens were immediately covered with plastic wrap until testing to mitigate excessive moisture loss.

Elastic modulus testing was exclusively carried out by participants 6 and 7, and the findings are shown in Fig. 14. The results indicated a time-dependent increase in elastic modulus for GGBFS-based AAC (M2) across all curing ages, with most stiffness development occurring within the first 28 days (see Fig. 9). A substantial increase was observed by 3 days, with both participants reaching the elastic modulus of approximately 27 GPa. By 7 days, the elastic modulus approached values close to the 28 days, highlighting a rapid early-age hardening of the GGBFS-based AAC mix. Comparatively, participant 6 generally exhibited

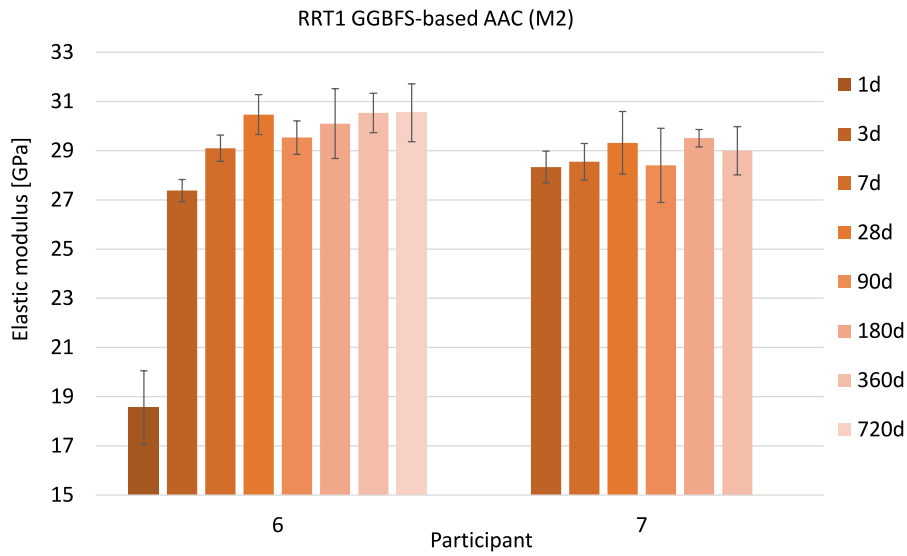

Fig. 14 Elastic modulus results for RRT1 GGBFS-based AAC (M2)

slightly higher elastic modulus values at early ages (3 to 28 days) than participant 7. However, both participants showed closely aligned values beyond 90 days, signifying reliability in the long-term mechanical properties.

The error bars, which reflect measurement variability, were more pronounced at early ages, particularly at 1 day, and gradually narrowed over time. This trend suggests that early-age measurements may be more sensitive to minor environmental or procedural variations, while the later stages reflect stable, reproducible properties as the GGBFS-based AAC fully cures. Participant 7 demonstrated slightly lower values compared to participant 6, correlating with the lower compressive strength values. However, the difference is not significant compared to the error bars of the data.

References

1. EN 197-1:2011 Cement - Part 1: Composition, specifications and conformity criteria for common cements. European Committee for Standardization (CEN), Brussels, Belgium, 2011.
2. EN 197-5:2021 Cement - Part 5: Portland-composite cement CEM II/C-M and Composite cement CEM VI. European Committee for Standardization (CEN), Brussels, Belgium, 2021.
3. Zivica V (2007) Effects of type and dosage of alkaline activator and temperature on the properties of alkali-activated slag mixtures. Constr Build Mater 21(7):1463–1469. https://doi.org/10.1016/j.conbuildmat.2006.07.002
4. Xu R, Kong F, Yang R, Wang H, Hong T (2024) Influences of silicate modulus and alkali content on macroscopic properties and microstructure of alkali-activated blast furnace slag-copper slag. Constr Build Mater 442:137622. https://doi.org/10.1016/j.conbuildmat.2024.137622
5. Zhang J, Shi C, Zhang Z (2021) Effect of Na_2O concentration and water/binder ratio on carbonation of alkali-activated slag/fly ash cements. Constr Build Mater 269:121258. https://doi.org/10.1016/j.conbuildmat.2020.121258
6. Provis JL, Arbi K, Bernal SA, Bondar D, Buchwald A, Castel A, Chithiraputhiran S, Cyr M, Dehghan A, Dombrowski-Daube K, Dubey A, Ducman V, Gluth GJG, Nanukuttan S, Peterson K, Puertas F, van Riessen A, Torres-Carrasco M, Ye G, Zuo Y (2019) RILEM TC 247-DTA round robin test: mix design and reproducibility of compressive strength of alkali-activated concretes. Mater Struct 52(5):99. https://doi.org/10.1617/s11527-019-1396-z
7. Xie T, Visintin P, Zhao X, Gravina R (2020) Mix design and mechanical properties of geopolymer and alkali activated concrete: review of the state-of-the-art and the development of a new unified approach. Constr Build Mater 256:119380. https://doi.org/10.1016/j.conbuildmat.2020.119380
8. Patil AA, Chore HS, Dodeb PA (2014) Effect of curing condition on strength of geopolymer concrete. Adv Concr Constr 2(1):29–37. https://doi.org/10.12989/ACC.2014.2.1.029
9. Nedunuri ASSS, Muhammad S (2024) Improving the workability and workable time of sodium hydroxide-activated ground granulated blast furnace slag binder-based concrete. Cement 16:100106. https://doi.org/10.1016/j.cement.2024.100106
10. Sun M, Mao X, Gao X, Lin Y, Li K, Zou C (2024) Innovative encapsulation of alkali activators in alkali-activated slag concrete: a sustainable strategy for

regulating setting time and durability. Constr Build Mater 427:136230. https://doi.org/10.1016/j.conbuildmat.2024.136230
11. Provis JL, van Deventer JSL (2014) Alkali activated materials. State-of-the-Art Report RILEM TC 224-AAM, Springer: Dordrecht, 2014, p 388. https://doi.org/10.1007/978-94-007-7672-2.
12. Tong S, Yuqi Z, Qiang W (2021) Recent advances in chemical admixtures for improving the workability of alkali-activated slag-based material systems. Constr Build Mater 272:121647. https://doi.org/10.1016/j.conbuildmat.2020.121647
13. Ma J, Dehn F (2017) Shrinkage and creep behavior of an alkali-activated slag concrete. Struct Concr 18(5):801–810. https://doi.org/10.1002/suco.201600147
14. Humad AM, Provis JL, Habermehl-Cwirzen K, Rajczakowska M, Cwirzen A (2021) Creep and long-term properties of alkali-activated Swedish-slag concrete. J Mater Civ Eng. https://doi.org/10.1061/(ASCE)MT.1943-5533.000338
15. Li Z, Delsaute B, Lu T, Kostiuchenko A, Staquet S, Ye G (2021) A comparative study on the mechanical properties, autogenous shrinkage and cracking proneness of alkali-activated concrete and ordinary Portland cement concrete. Constr Build Mater 292:123418. https://doi.org/10.1016/j.conbuildmat.2021.123418
16. Collins F, Sanjayan JG (2001) Microcracking and strength development of alkali activated slag concrete. Cem Concr Compos 23(4):345–352. https://doi.org/10.1016/S0958-9465(01)00003-8
17. Lee NK, Lee HK (2013) Setting and mechanical properties of alkali-activated fly ash/slag concrete manufactured at room temperature. Constr Build Mater 47:1201–1209. https://doi.org/10.1016/j.conbuildmat.2013.05.107
18. Collins FG, Sanjayan JG (1999) Workability and mechanical properties of alkali activated slag concrete. Cem Concr Res 29(3):455–458. https://doi.org/10.1016/S0008-8846(98)00236-1
19. Jittin V, Madhuri P, Santhanam M, Bahurudeen A (2021) Influence of preconditioning and curing methods on the durability performance of alkali-activated binder composites. Constr Build Mater 311:125346. https://doi.org/10.1016/j.conbuildmat.2021.125346
20. Sofi M, van Deventer JSJ, Mendis PA, Lukey GC (2007) Engineering properties of inorganic polymer concretes (IPCs). Cem Concr Res 37(2):251–257. https://doi.org/10.1016/j.cemconres.2006.10.008
21. Al-Otaibi S (2008) Durability of concrete incorporating GGBS activated by water-glass. Constr Build Mater 22(10):2059–2067. https://doi.org/10.1016/j.conbuildmat.2007.07.023
22. Li N, Shi C, Zhang Z, Zhu D, Hwang H-J, Zhu Y, Sun T (2018) A mixture proportioning method for the development of performance-based alkali-activated slag-based concrete. Cem Concr Compos 93:163–174. https://doi.org/10.1016/j.cemconcomp.2018.07.009
23. EN 12390-6:2024 Testing hardened concrete part 6: Tensile splitting strength of test specimens. European Committee for Standardization (CEN), Brussels, Belgium, 2024.
24. ASTM C496/C496M-17 Standard test method for splitting tensile strength of cylindrical concrete specimens, American Society for Testing and Materials: West Conshohocken, PA, USA, 2017.
25. ASTM C78/C78M-18 Standard Test. Method for flexural strength of concrete (using simple beam with third-point loading); American Society for Testing and Materials: West Conshohocken, PA, USA, 2018.
26. EN 12390-5:2019 Testing hardened concrete. Flexural strength of test specimens. European Committee for Standardization (CEN), Brussels, Belgium, 2019.
27. Yang K-H, Cho A-R, Song J-K (2012) Effect of water–binder ratio on the mechanical properties of calcium hydroxide-based alkali-activated slag concrete. Constr Build Mater 29:504–511. https://doi.org/10.1016/j.conbuildmat.2011.10.062
28. Yurt U (2020) High performance cementless composites from alkali activated GGBFS. Constr Build Mater 264:120222. https://doi.org/10.1016/j.conbuildmat.2020.120222
29. Collins F, Sanjayan JG (1998) Early age strength and workability of slag pastes activated by NaOH and Na_2CO_3. Cem Concr Res 28(5):655–664. https://doi.org/10.1016/S0008-8846(98)00025-8
30. Amer I, Kohail M, El-Feky MS, Rashad A, Khalaf MA (2021) A review on alkali-activated slag concrete. Ain Shams Eng J 12(2):1475–1499. https://doi.org/10.1016/j.asej.2020.12.003
31. Bezemer HJ, Awasthy N, Lukovic M (2023) Multiscale analysis of long-term mechanical and durability behaviour of two alkali-activated slag-based types of concrete. Constr Build Mater 407:133507. https://doi.org/10.1016/j.conbuildmat.2023.133507
32. Matalkah F, Ababneh A, Aqel R (2022) Effects of nanomaterials on mechanical properties, durability characteristics and microstructural features of alkali-activated binders: a comprehensive review. Constr Build Mater 336:127545. https://doi.org/10.1016/j.conbuildmat.2022.127545
33. Younus SJ, Mosaberpanah MA, Alzeebaree R (2023) The performance of alkali-activated self-compacting concrete with and without nano-alumina. Sustainability 15(3):2811
34. Rossi L, Miranda de Lima L, Sun Y, Dehn F, Provis JL, Ye G, De Schutter G (2022) Future perspectives for alkali-activated materials: from existing standards to structural applications. RILEM Tech Lett 7:159–177
35. Ding Y, Dai J-G, Shi C-J (2016) Mechanical properties of alkali-activated concrete: a state-of-the-art review. Constr Build Mater 127:68–79. https://doi.org/10.1016/j.conbuildmat.2016.09.121
36. Hassan A, Arif M, Shariq M (2019) Use of geopolymer concrete for a cleaner and sustainable environment – a review of mechanical properties and microstructure. J Clean Prod 223:704–728. https://doi.org/10.1016/j.jclepro.2019.03.051
37. ACI 318-19 (2022) Building code requirements for structural concrete. American Concrete Institute, MI, USA.
38. Thomas RJ, Peethamparan S (2015) Alkali-activated concrete: engineering properties and stress–strain behavior.

Constr Build Mater 93:49–56. https://doi.org/10.1016/j.conbuildmat.2015.04.039
39. Kara De Maeijer P, Ramagiri KK, Lukovic M, Rossi L, Masi G, Kar A, Ganapathi Chottemada P, Yliniemi J, Ichimiya K, Sha W, Dehn F, Ye G Chapter 7. Hardened AAM properties. In: Ye G, Dehn F (eds) Mechanical properties of alkali-activated concrete. RILEM State-of-the-Art Reports. Springer (in submission).
40. Sun Y, Dai X, Sun B, Attupurathu Vijayan R, Tao Y, Yliniemi Y, Gao M, Sha W, Palacios M, Puertas F, De Schutter G Chapter 6. Fresh AAM properties. In: Ye G, Dehn F (eds) Mechanical properties of alkali-activated concrete. RILEM State-of-the-Art Reports. Springer (in submission).
41. EN 12620 Aggregates for concrete. European Committee for Standardization (CEN), Brussels, Belgium, 2016.
42. ASTM C33/ C33M-18 Standard specification for concrete aggregates, ASTM International, West Conshohocken, PA, USA, 2018.
43. EN 206:2013 Concrete: specification, performance, production and conformity. European Committee for Standardization (CEN), Brussels, Belgium, 2013.
44. EN 12350-2 Testing fresh concrete - Part 2: Slump test. European Committee for Standardization (CEN), Brussels, Belgium, 2019.
45. ASTM C143/C143M-20 Standard test method for slump of hydraulic-cement concrete. ASTM International: West Conshohocken, PA, USA, 2020.
46. EN 12350-5 Testing fresh concrete - Part 5: Flow table test. European Committee for Standardization (CEN), Brussels, Belgium, 2019.
47. ASTM C1621/C1621M-17 Standard test method for passing ability of self-consolidating concrete by J-Ring. ASTM International: West Conshohocken, PA, USA, 2017.
48. Sun Y, Mohan MK, Dai X, Zhang Y, Ye G, De Schutter G (2024) Effects of mixing conditions and activator anionic species on the rheology of silicate-activated slag concrete. Cem Concr Compos 150:105556. https://doi.org/10.1016/j.cemconcomp.2024.105556
49. EN 12390-7:2019/AC:2020 Testing hardened concrete - Part 7: Density of hardened concrete. European Committee for Standardization (CEN), Brussels, Belgium, 2020.
50. ASTM C138 / C138M - 17a Standard test method for density (unit weight), yield, and air content (gravimetric) of concrete. ASTM International, West Conshohocken, PA, USA, 2023.
51. EN 12390-3 Testing hardened concrete - Part 3: Compressive strength of test specimens. European Committee for Standardization (CEN), Brussels, Belgium, 2019.
52. ASTM C39/C39M-21 Standard test method for compressive strength of cylindrical concrete specimens. American Society for Testing and Materials: West Conshohocken, PA, USA, 2021.
53. LVS 156-1:2022 Concrete. Latvian National Annex to European Standard EN 206 Concrete. Technical provisions, performance,manufacture and compliance [Latvijas nacionālais pielikums Eiropas standartam EN 206 Betons. Tehniskie noteikumi, darbuizpildījums, ražošana un atbilstība (in Latvian)], Cabinet of Ministers, Latvia, 2023.
54. Mavroulidou M, Sanam I, Mengasini L (2023) Mechanical and durability performance of alkali-activated slag cement concretes with carbonate and silicate activators. Sustain Chem Pharm 31:100896. https://doi.org/10.1016/j.scp.2022.100896
55. Fernandez-Jimenez A, Puertas F (2001) Setting of alkali-activated slag cement. Influence of activator nature. Adv Cem Res 13(3):115–121
56. Bokan Bosiljkov V, Kramar Fijavz M, Serdar M (2018) Mechanical properties of cement based materials - extended Round Robin Test of COST Action TU 1404. Proceedings of SynerCrete'18 - Interdisciplinary Approaches for Cement-based Materials and Structural Concrete: Synergizing Expertise and Bridging Scales of Space and Time, 24 -26 October 2018 Funchal, Portugal, 47–54.
57. Koehler EP, Fowler DW (2004) Development of a portable rheometer for fresh Portland cement concrete. Research report ICAR 105–3F, The University of Texas at Austin, TX, USA, p. 306. https://repositories.lib.utexas.edu/server/api/core/bitstreams/e7126ff0-f9df-4771-8ed0-2bf1e3b0f5e4/content. Accessed 21 March 2024.
58. Feys D, Wallevik JE, Yahia A, Khayat KH, Wallevik OH (2013) Extension of the Reiner-Riwlin equation to determine modified Bingham parameters measured in coaxial cylinders rheometers. Mater Struct 46(1):289–311
59. EN 12390-13 Testing hardened concrete - Part 13: Determination of secant modulus of elasticity in compression. European Committee for Standardization (CEN), Brussels, Belgium, 2021.
60. ASTM C469 / C469M - 14e1 Standard test method for static modulus of elasticity and Poisson's ratio of concrete in compression. ASTM International, West Conshohocken, PA, USA, 2022.